Available online at www.sciencedirect.com
ScienceDirect
Cement & Concrete Composites 29 (2007) 103–116
Cement & Concrete Composites
www.elsevier.com/locate/cemconcomp

Numerical tests of thermal cracking induced by temperature gradient in cement-based composites under thermal loads

Y.F. Fu [a], Y.L. Wong [b,*], C.S. Poon [b], C.A. Tang [c]

[a] Research Institute of Highway, MOC, Beijing 100088, PR China
[b] The Hong Kong Polytechnic University, Hung Hom, Kowloon, Hong Kong, PR China
[c] Dalian University of Technology, School of Civil and Hydraulic Engineering, Dalian 116024, PR China

Received 27 October 2005; received in revised form 31 August 2006; accepted 1 September 2006
Available online 1 November 2006

Abstract

This paper presents the development of a new method to model the thermal stresses and cracks in a heterogeneous cement-based composite material under elevated temperature. Numerical case studies were performed to determine the effects of temperature gradient, heating rate, and variable coefficient of thermal expansion and heterogeneity of materials on the thermal stresses and associated cracking in a cement-based composite material exposed to a transient thermal load. It is found that (1) the settling time and the temperature difference between the surface and the center of specimen increase with the heating rate; (2) the thermal stresses increase with temperature difference, but remain constant if the temperature difference only increases uniformly; (3) most of the cracks induced by temperature gradient are formed before the settling time, and thereafter the thermal mismatch-induced cracks continue to propagate; (4) uncertainties of the occurrence of explosive spalling are probably caused by the thermally induced cracks and the heterogeneities of the constitute materials.

Keywords: Temperature gradient; Thermally induced cracks; Heterogeneity; Explosive spalling; Numerical simulation

1. Introduction

Research studies on fire resistance properties of normal strength concrete (NSC) commenced in early twenties, and the results formed the basis of many current structural fire design codes of concrete [1]. The effects of high temperatures on high strength concrete (HSC) (with compressive strength >60 MPa) have also been extensively studied since the past decade [2]. Although there are significant differences between NSC and HSC in terms of fire performance, the nature of thermal damages (crack formation, explosive spalling, degradation of mechanical/durability properties) are similar, and they mainly arise from (i) thermal mismatch within the concrete material, (ii) decomposition of cementitious hydrates, and (iii) the build up of pore pressure due to the vaporization of pore water.

Regarding the thermal mismatch, the thermal stresses developed in concrete are caused by (i) the incompatibility of the coefficients of thermal expansion (CTE) of the constitutive materials in the concrete and (ii) the temperature gradient generated across the concrete section. The higher the heating rate, the steeper will be the temperature gradient. It was found that as the heating rate increased, the frequency of the concrete having spalling damages increased, but the extent of the spalling damages was reduced [3,4]. For instance, tests on HSC revealed [4] that under a low furnace heating rate of 2 °C/min, the test concrete cubes were burst into small fragments by explosive spalling. On the other hand, using the ISO standing fire heating rate in which the initial temperature rise was about 100 °C/min, the spalling damage was characterized by breaking off of the corners of the cubes leaving the cores of the cube

* Corresponding author. Tel.: +852 27666009; fax: +852 23346389.
E-mail address: ceylwong@polyu.edu.hk (Y.L. Wong).

0958-9465/$ - see front matter © 2006 Published by Elsevier Ltd.
doi:10.1016/j.cemconcomp.2006.09.002

Nomenclature

α	coefficient of thermal expansion	λ	ratio of tensile strength to compressive strength
ϕ	density function of mechanical property	θ	friction angle
β	scale parameter	k_x,k_y	heat conductivity in direction x and y
β_0	mean value of β	k_0	original value of heat conductivity
h	shape parameter	ρ	material density
RVE	representative volume element	c	specific heat
σ	thermal stress	ω	residual coefficient of heat conductivity
σ_r	residual stress after peak-strength	Γ_s	boundary conditions on surface area
D	damage variable	Ω	domain
D_T	thermo-mechanical damage	$[K_e]$	element heat conductivity matrix
D_m	thermo-dehydrated damage	$[C_e]$	element heat capacitance matrix
m_h	hydrate mass	$[F_e]$	element thermal force matrix
ε	strain induced by internal and external restriction	$[B]$	geometry matrix
		$[D]$	conductivity matrix
$\varepsilon_{thermal}$	initial strain at temperature increment of ΔT	$[N]$	shape function
ε_σ	stress-induced strain	Δt	time interval
E^0	initial elastic modulus	Q	internal heat source
$E^{0'}$	elastic modulus at temperature T'	CTE	coefficient of thermal expansion
ΔT	temperature increment	q	heat flux
ξ	coefficient of residual strength	HCP	hardened cement paste
S	peak-strength	t_s	settling time
S_r	residual strength	σ_x	horizontal stress
S_c	uniaxial compressive strength	σ_y	vertical stress
S_t	uniaxial tensile strength		

intact. Thus, the heating rate or the temperature gradient is one of the key factors dictating the thermal damage of the concrete or the fire performance of reinforced concrete structures. This damage mechanism needs to be adequately quantified both experimentally and analytically.

Back in the early seventies, Timoshenko and Goodier [5] proposed an analytical solution to describe the internal stresses in a homogeneous and isotropic solid cylinder subjected to rapid heating. Similar finite difference analyses were conducted by Khoury et al. [6]. It was concluded that the thermal diffusivity, the heating rate and the dimension of the specimen were the main factors affecting the temperature gradient and stress distribution. Further to the Timoshenko and Goodier's formula and Carslaw and Jaeger's study [7], Kristensen et al. [8] developed a modified analytical expression for the thermally induced stresses in hardened cement paste (HCP) and concrete under thermal shock. Numerical software packages [9] were also developed to model the effect of high temperature on concrete. These packages typically were consisted of two separate but connected thermal and mechanical programs so that the temperature field output of the thermal software could be used as input into the mechanical property software at every time step to produce the strain/stress results. However, most of these packages did not simulate the changes in the heat flow due to the formation of cracks. They also could not model the random nature of crack formation due to the inherent heterogeneity of the constitutional materials of the concrete. Recently, Khoury et al. [10] developed an advanced HITECO model package that fully coupled the thermal, chemical and mechanical formulations of concrete. It incorporated the effects of chemical–physical phase changes and the effects of changes on permeability and non-linearities due to temperature and pressure. Although the complex HITECO model is conceptually sound, there are practical problems to isolate and realistically quantify the parameters in the mathematical formulae for each effect.

Recently the authors of this paper proposed a mechanical thermal-elastic damage (MTED) model to investigate thermal cracks induced by thermal mismatches and heterogeneities in a cement-based composite under a uniform temperature field [11,12]. As an extension of the previous work, the MTED model was modified to account for the degradation of the mechanical properties of the composite materials as a function of temperature, and a 2-D transient heat transfer program was also developed to calculate the temperature gradient. The heat transfer program was then integrated into the modified MTED model to form a new software package *T*-MFPA (temperature version of material fracture process analysis). This paper describes the basic formulation of the *T*-MFPA package, and discusses the effects of temperature gradient on the change of thermal stresses, cracking processes and crack patterns of a cement-based composite through numerical case studies.

2. Formulation of *T*-MFPA program

2.1. Material model

Concrete is a multiple-phase heterogeneous material. In this paper, in order to study the thermal cracking process induced by thermal mismatches and temperature gradient, concrete is regarded as a two-phase material (mortar matrix and inclusion), in which all phase materials are heterogeneous. In order to develop a random distribution of material heterogeneity, a statistical approach is used. The probability functions (such as normal distribution function, Weibull distribution function) can be adopted to represent the random characteristics of material properties [13] (elastic modulus, compressive strength, Poisson's ratio). The Weibull distribution (purely empirical function) is a widely adopted function in reliability engineering (such as material strength). Since the material heterogeneity is characterized by the spatial scatter of the material properties, the Weibull distribution is selected to represent the meso-scale heterogeneity of the phase materials in this study. A 2-parameter probability density function (PDF) of the general Weibull distribution is given by

$$\varphi(h,\beta)=\frac{h}{\beta_0}\times\left(\frac{\beta}{\beta_0}\right)^{h-1}\times \mathrm{e}^{-\left(\frac{\beta}{\beta_0}\right)^{h}}\beta,\quad \beta_0\geqslant 0;\quad h>0 \tag{1}$$

where h is the shape parameter (or slope); β_0 is the scale parameter. $\varphi(\beta)$ is the density of variable β. With increasing h value, the phase material becomes more homogeneous.

2.2. Thermal conduction

Neglecting the coupling term, the Fourier partial differential equation for transient thermal conduction in two-dimension can be expressed as [14]:

$$\frac{\partial}{\partial x}k_x\frac{\partial T(x,y,t)}{\partial x}+\frac{\partial}{\partial y}k_y\frac{\partial T(x,y,t)}{\partial x}+Q(x,y,t)=\rho c\frac{\partial T}{\partial t} \tag{2}$$

where k_x and k_y are the thermal conductivities in the x- and y-directions respectively; $Q(x,y,t)$ is the heat generation by the material per unit volume and time; ρ is the material density; c is the specific heat of the material. ρ and c are treated as stress-independent. In this study, the thermal conductivity is considered as a temperature-dependent and isotropic constant (i.e. its value is dependent on the temperature and the imposed stress state after peak-strength). It is assumed that when a fractured element is in tension, the thermal conductivity is similar to that of air; while it has a residual value of its original one when it is in compression. Hence, the thermal conductivity of the material after fracture can be expressed as

$$k=\omega k_0\begin{cases}\omega=0 & \text{in tension}\\ \omega=1 & \text{in compression}\end{cases} \tag{3}$$

where k_0 is the original value of the thermal conductivity; ω is the residual coefficient. Since no experimental technique is available to measure the residual coefficient, we assign 0 and 1 for conditions of tension and compression respectively. In order to solve Eq. (2), it is necessary to specify the initial condition at time $t=t_0$ in the domain Ω and the boundary conditions on the surface Γ_s. In this study, the initial temperature distribution $T_0(x,y)$ is assigned with a constant value for the uniform temperature conditions and it can be mathematically expressed as follows:

$$T(x,y,t_0)=T_0(x,y)\quad t_0=0 \text{ in } \Omega \tag{4}$$

The temperature of surface Γ_s is a function of time and can be written as

$$T=T(x,y,t)\quad T>0 \text{ on } \Gamma_s \tag{5}$$

Accordingly, the finite element formulation of Eq. (2) can be re-written as

$$[C_e]\{\dot{T}(t)\}+[K_e]\{T(t)\}=\{F_e\} \tag{6}$$

where $[K_e]=\int_v[B]^T[D][B]\mathrm{d}v$, element heat conductivity matrix; $[C_e]=\int_v\rho c[N]^T[N]\mathrm{d}v$, element heat capacitance matrix; $[F_e]=\int_v Q[N]\mathrm{d}v-\int_s\{q\}^T\{n\}[N]\mathrm{d}s$, element thermal force matrix; where $[B]$, $[D]$ and $[N]$ are the geometry matrix, the conductivity matrix, and the shape function respectively. Q is an internal heat source and q is the heat flux.

Using the backward difference scheme of a two-level explicit method [15], Eq. (6) can be expressed by the following finite element equation for transient heat conduction

$$\left([K_e]+\frac{[C_e]}{\Delta t}\right)\{T\}_t=\{F_e\}_t+\frac{[C_e]}{\Delta t}\{T\}_{t-\Delta t} \tag{7}$$

where Δt is a given time interval; $\{T\}_{t-\Delta t}$ is the given temperature at a prescribed time $t-\Delta t$. $\{T\}_t$ is the unknown temperature at time t. It is clear that an iteration scheme is employed to resolve the expected temperature $\{T\}_t$ through the given temperature $\{T\}_{t-\Delta t}$.

2.3. Bilinear mesoscopic thermo-elastic damage model

It is essential to consider the coupling and non-linearity of all the processes involved in the degradation mechanism of a heated concrete. There are a number of factors that cause such damages, such as thermal mismatches between the materials, temperature gradients, the decomposition of hydration products, and the build up of pore water pressure. The buildup of vapor pressure is closely related to the moisture content [16] and the permeability of concrete which are dependent on crack formation [17]. It is desirable to establish a model to trace the crack formation and propagation processes.

Based on the above-mentioned damage mechanisms [18], a general form of thermally induced stress for a given state of damage for a representative volume element (RVE) can be expressed as follows:

$$\sigma(\varepsilon, \Delta T) = [1 - D]E^0(\varepsilon - \varepsilon_{\text{thermal}}) \tag{8}$$

Strain ε is equal to the sum of ε_σ and $\varepsilon_{\text{thermal}}$. ε_σ is the stress-induced strain ($\varepsilon_\sigma = \varepsilon - \varepsilon_{\text{thermal}}$). $\varepsilon_{\text{thermal}}$ is the thermal strain at temperature increment of ΔT and is equal to $\alpha\Delta T$. Under a thermal loading, the damage is induced both by the differential thermal strains and the dehydration due to the temperature increment ΔT. The general expression of the damage variable is $D = D(\varepsilon_\sigma, \Delta T)$. Let D_{m} and D_T denote the scalar variables of thermo-mechanical damage and thermo-dehydrated damage respectively. If they are independent, the damage variable $D(\varepsilon_\sigma, \Delta T)$ can be expressed as

$$D(\varepsilon_\sigma, \Delta T) = 1 - (1 - D_{\text{m}})(1 - D_{\text{T}}) \tag{9}$$

The thermo-mechanical damage variable is assumed to be a function of the stiffness degradation, i.e.

$$D_{\text{m}} = 1 - \frac{E(\varepsilon_\sigma)}{E^0} \tag{10}$$

E^0 is the elastic modulus in a reference/undamaged condition. A linear elastic damage model was introduced to determine the damage variable D_{m}. The readers are referred to the literatures for detailed description of this expression [11].

Essentially, the degradation of the elasticity modulus due to the thermo-chemical reaction should be expressed as

$$D_{\text{T}} = 1 - \frac{E(m_{\text{h}})}{E^0} \tag{11}$$

where m_{h} is the mass of the hydration products; $E(m_{\text{h}})$ is the elastic modulus at the mass of hydration products equal to m_{h}. The proportion $f(m_{\text{h}}) = \frac{E(m_{\text{h}})}{E^0}$ can be regarded as the degree of hydration, so that dehydration can be expressed as $1 - f(m_{\text{h}})$. This is an intrinsic property of concrete. Experiments have shown that the content of hydration products m_{h} is reduced with increasing temperature. Thus, the hydration degree $f(m_{\text{h}})$ is also a function of temperature, namely $f(m_{\text{h}}) = f_E(T) = \frac{E(T)}{E^0}$. Based on SEM experimental results [19], the relationship $f_E(T)$ between the elastic modulus and the temperature can be determined. Substituting Eqs. (10) and (11) into Eq. (9), we can obtain another expression of the general damage:

$$D(\varepsilon_\sigma, \Delta T) = 1 - \frac{E(\varepsilon_\sigma)}{E^0}\frac{E(\Delta T)}{E^0} \tag{12}$$

This model covers the effects of external loadings and elevated temperatures, as discussed hereafter.

As discussed earlier, the total strain ε is assumed to consist of the thermal strain $\varepsilon_{\text{thermal}}$ and the stress-inducing mechanical strain ε_σ, and can be expressed by

$$\varepsilon = \varepsilon_{\text{thermal}} + \varepsilon_\sigma \tag{13}$$

The stress σ for a given total strain ε at a temperature T can be determined according to the stress–strain curves (see Fig. 1).

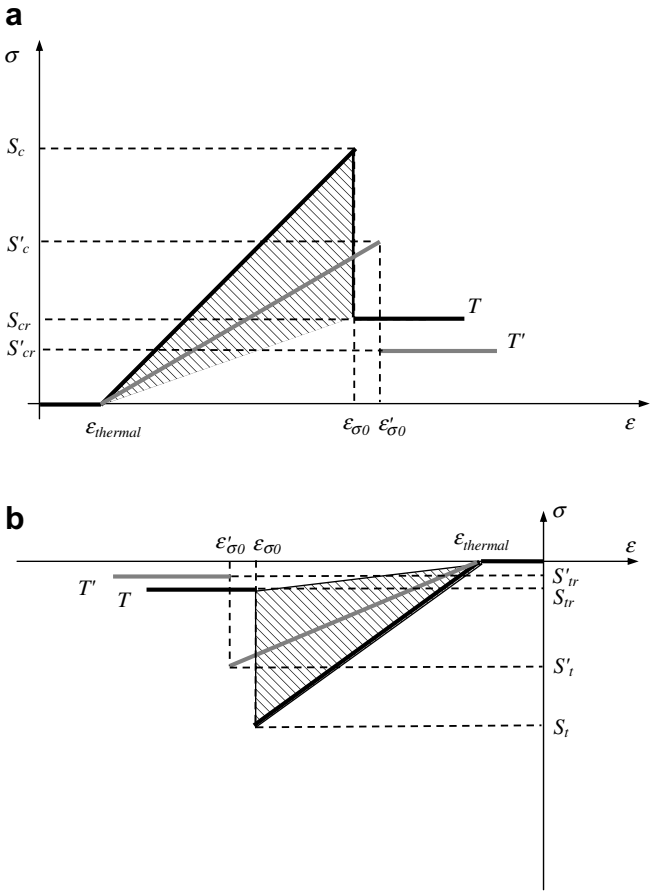

Fig. 1. Bi-linear temperature-dependent constitutive behavior of RVE: (a) Constitutive behavior of RVE under compression; (b) constitutive behavior of RVE under tension.

$$\sigma = \begin{cases} E^0(\varepsilon - \varepsilon_{\text{thermal}}) & \sigma \leqslant S_{\text{c}} \quad \text{or } S_t \\ \sigma_{\text{r}} & \sigma > S_{\text{c}} \quad \text{under compression} \\ 0 & \sigma < S_t \quad \text{under tension} \end{cases} \tag{14}$$

where σ_{r} is the residual stress after peak-strength; $\sigma_{\text{r}} = \xi S_{\text{c}}$ at a given temperature T; ξ is the coefficient of residual strength. The relation $E(\varepsilon)$ between the elastic modulus and the strain at a given temperature is as follows:

$$E(\varepsilon) = \begin{cases} E^0 & \sigma \leqslant S_{\text{c}} \text{ or } S_t \\ \xi\frac{\varepsilon_{\sigma 0} - \varepsilon_{\text{thermal}}}{\varepsilon - \varepsilon_{\text{thermal}}}E^0 & \sigma > S_{\text{c}} \text{ under compression} \\ 0 & \sigma < S_t \text{ under tension} \end{cases} \tag{15}$$

According to Mazars' [20] and Yu's [21] descriptions of the damage process, the thermal induced damage before and after the peak-strength can be determined by the thermal strain and the temperature T through a separation function respectively. Fig. 1 shows a general constitutive relationship of a RVE under thermal loading. The damage at any given thermal strain ε and temperature T can be calculated from Eq. (16)

$$D(\varepsilon,T)=\begin{cases}1-f_E(T) & \varepsilon_{\text{thermal}}\leqslant\varepsilon\leqslant\varepsilon_{\sigma 0}\\ 1-\frac{\xi(\varepsilon_{\sigma 0}-\alpha\Delta T)}{(\varepsilon-\alpha\Delta T)}f_E(T) & \varepsilon\geqslant\varepsilon_{\sigma 0}\text{ under compression}\\ 1 & \varepsilon\geqslant\varepsilon_{\sigma 0}\text{ under tension}\end{cases}\tag{16}$$

where $D(\varepsilon,T)$ represents the thermal damage with respect to the thermal strain ε and the temperature T; ε_σ is the stress-induced strain; $\varepsilon_{\sigma 0}$ is the strain at peak-strength; Under compression, ξ is less than 1 but greater than 0. Under tension, ξ is equal to 0. In case of $f_E(T)=1$, and when the strain ε becomes smaller than or equal to $\varepsilon_{\sigma 0}$, the RVE is undamaged and intact, so that $D=0$. When the strain ε is larger than $\varepsilon_{\sigma 0}$, and under a compressive state, the RVE is damaged, i.e. $D>0$, and the damage variable shall be calculated by the residual strength. Under a tensile state, the RVE is fully damaged and does not sustain any load, and $D=1$. In case of $f_E(T)<1$, even though the strain ε is less than $\varepsilon_{\sigma 0}$, the RVE is damaged due to the decomposition of hydration products. When the strain ε is larger than $\varepsilon_{\sigma 0}$ and is under compression, the RVE is damaged both by the temperature increment and by the increased strain. Since the thermally induced stress at a given strain ε and temperature T can be determined by Eq. (8), and by substituting Eq. (16) into Eq. (8), a mesoscopic non- local damage model, which can describe the complete thermal induced damage process, is expressed as

$$\sigma=\begin{cases}f_E(T)E^0(\varepsilon-\alpha T) & \varepsilon_{\text{thermal}}\leqslant\varepsilon\leqslant\varepsilon_{\sigma 0}\\ \xi f_E(T)E^0(\varepsilon_{\sigma 0}-\alpha T) & \varepsilon\geqslant\varepsilon_{\sigma 0}\text{ under compression}\\ 0 & \varepsilon\geqslant\varepsilon_{\sigma 0}\text{ under tension}\end{cases}\tag{17}$$

Similarly, the elastic modulus at a given total strain ε and temperature T can be obtained as follows:

$$E(\varepsilon,T)=\begin{cases}f_E(T)E^0 & \varepsilon_{\text{thermal}}\leqslant\varepsilon\leqslant\varepsilon_{\sigma 0}\\ \frac{\xi(\varepsilon_{\sigma 0}-\alpha\Delta T)}{(\varepsilon-\alpha\cdot\Delta T)}f_E(T)E^0 & \varepsilon\geqslant\varepsilon_{\sigma 0}\text{ under compression}\\ 0 & \varepsilon\geqslant\varepsilon_{\sigma 0}\text{ under tension}\end{cases}\tag{18}$$

Let $E^{0'}=f_E(T)E^0$, and $E^{0'}$ can be regarded as the elastic modulus at temperature T'. The thermal stress in Eq. (17) has the same expression as the stress at room temperature, at which $f_E(T)$ is equal to 1. In case of plane problem, the aforementioned ultimate strains are determined as follows:

$$\varepsilon_{\sigma 0}=\begin{cases}\frac{1}{E^0}\left(\frac{1+\sin\theta}{1-\sin\theta}\sigma_2+S_c-\mu\sigma_2\right) & \text{under compression}\\ \frac{S_t}{E^0} & \text{under tension}\end{cases}\tag{19}$$

where $S_t=-\lambda S_c$ and λ is the ratio of tensile strength to compressive strength. S_t and S_c are uniaxial tensile strength and compressive strength respectively. θ is the friction angle of the material. Both the compressive strength and the tensile strength are temperature-dependent, and can be determined based on the experimental results [19]. In this study, we consider a compressive stress is positive and a tensile stress is negative.

In the bilinear temperature-dependent damage model shown in Fig. 1, a strength-based criterion is adopted to model the cracking process. It is assumed that the stress–strain relationship of a RVE is linearly elastic till its peak-strength is reached, and thereafter follows a drop to its residual strength. The broken RVE can be considered as a fine crack. Cracking is treated as a smeared phenomenon. That is, a crack is not considered as a discrete displacement jump, but rather the properties of the RVE are supposed to be changed according to a continuum law, such as damage mechanics. The behavior laws of RVE are implemented by introducing the mesoscopic thermo-elastic damage variable D into the above-mentioned constitutive relationship.

A linear 2-D FEM program is developed to calculate the thermal stresses, in which a quadrilateral element with four nodes is adopted to discretize the given object in the FEM analysis. Work is underway to simulate thermally induced crack growth using 3-D models of concrete materials.

3. Verification and numerical case studies

The calculated temperature gradient and thermal stress field by T-MFPA were in good agreement with those reported by Logan [22]. This confirms the correctness and the reliability of the results calculated using the proposed T-MFPA package [23].

In order to study the effects of heating rate, temperature gradient and coefficient of thermal expansion (CTE) on the thermal stress and crack developments, eight numerical specimens consisted of three different simulated cement-based materials (as shown in Fig. 2) were used as case studies. The first simulated material was a homogeneous single-phase material (matrix), and was used in Cases "1" and "2", to investigate the effects of heating rate on the temperature gradient and thermal stresses. The second simulated material was a heterogeneous single-phase material (matrix), and was used in Cases "3", "4" and "5", to determine the effects of heating rate and variant CTE on thermal cracking. The last simulated material was a multi-phase material (matrix and inclusions), and was used in Cases "6", "7", and "8", to explore the effects of temperature gradient and temperature-dependent properties of the phase materials. The geometric and mechanical properties of the three materials are listed in Table 1.

In Cases "1" and "2", two heating rates of 10 °C/min and 20 °C/min were adopted. In Case "5", the function of CTE with respect to temperature for the single phase matrix (say hardened cement paste) is expressed as Eq. (20) which was determined by curve fitting of the experimental results [19].

$$\begin{aligned}\alpha(T)=&-2\times10^{-15}T^4+3\times10^{-12}T^3\\&-2\times10^{-9}T^2+3\times10^{-7}T-1\times10^{-6}\end{aligned}\tag{20}$$

In Case "8", the effects of temperature-dependent mechanical properties (S_c, S_t and E) were considered.

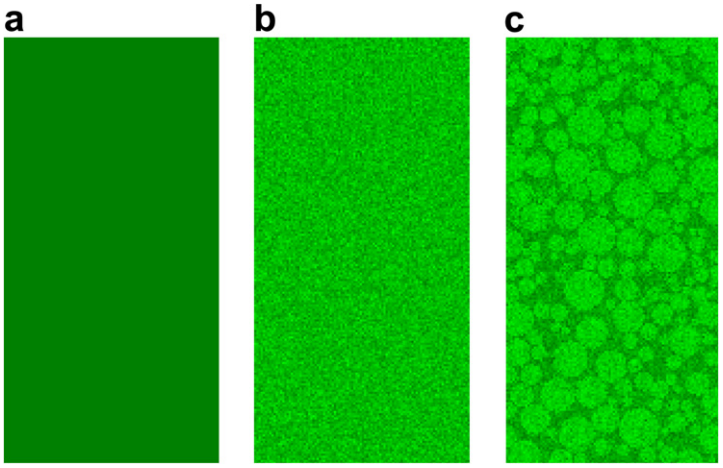

Fig. 2. Modeling materials 1–3. (a) Material 1; (b) material 2; (c) material 3.

Table 1
Geometrical and mechanical properties of specimens

Materials		Elastic modulus (GPa)		Compressive strength (MPa)		Poisson's ratio	CTE (°C)	Heat conductivity (W/m^{2}C)	Volume specific heat (J/m^{3}C)	Cases
		h	E_0	h	σ_0					
1		300	40	300	200	0.20	1.0E−5	1.8	1.93E+6	1,2
2		3	40	3	200	0.20	1.0E−5	1.8	1.93E+6	3,4,5
3	Matrix	3	40	3	200	0.20	Variant 1.0E−5	1.8	1.93E+6	6,7,8
	Inclusion	6	70	6	300	0.18	1.2E−5	3.0	1.20E+6	

The empirical functions of S_c and E at a given temperature T were taken as follows:

(1) Relationships between compressive strength and temperature matrix material (mortar)

$$\frac{S}{S_C} = -1.36 \times 10^{-3} T + 1.03 \tag{21}$$

Inclusion material (granite)

$$\frac{S}{S_C} = \begin{cases} 1 & 25^\circ\text{C} \leqslant T \leqslant 300\ ^\circ\text{C} \\ -2.27 \times 10^{-3} T + 1.68 & T > 300\ ^\circ\text{C} \end{cases} \tag{22}$$

(2) Relationships between elastic modulus and temperature matrix material (mortar)

$$\frac{E}{E_0} = \begin{cases} -2.91 \times 10^{-3} T + 1.07 & 25\ ^\circ\text{C} \leqslant T \leqslant 300\ ^\circ\text{C} \\ -3.33 \times 10^{-4} T + 0.30 & T > 300\ ^\circ\text{C} \end{cases} \tag{23}$$

Inclusion material (granite)

$$\frac{E}{E_0} = \begin{cases} -2.00 \times 10^{-3} T + 1.05 & 25\ ^\circ\text{C} \leqslant T \leqslant 300\ ^\circ\text{C} \\ -3.00 \times 10^{-4} T + 0.54 & T > 300\ ^\circ\text{C} \end{cases} \tag{24}$$

Strictly speaking, the heating conditions at the two ends of the numerical specimen were not necessarily the same as those at its surface. For the higher range of temperatures at above 200 °C, the temperatures at the specimen ends became closer to those of the curved surface. Thus, the numerical specimens were considered to be heated at uniform rates to 600 °C from all sides of the specimens without external loading. The same temperature was prescribed at all surfaces at any given time, and it increased linearly with time. All numerical simulations were performed under a plane-stress state without external loadings.

4. Numerical results

4.1. Heating rate

4.1.1. Temperature profile

The temperature distributions along the cross-sections of the specimens in Cases "1" and "2" at the heating rate of 10 °C/min and 20 °C/min respectively are plotted in Fig. 3. It is observed that temperature profile is steeper near the specimen surface with increasing heating rate. The corresponding calculated temperature differences ΔT between the centers and the surfaces of the specimens are given in

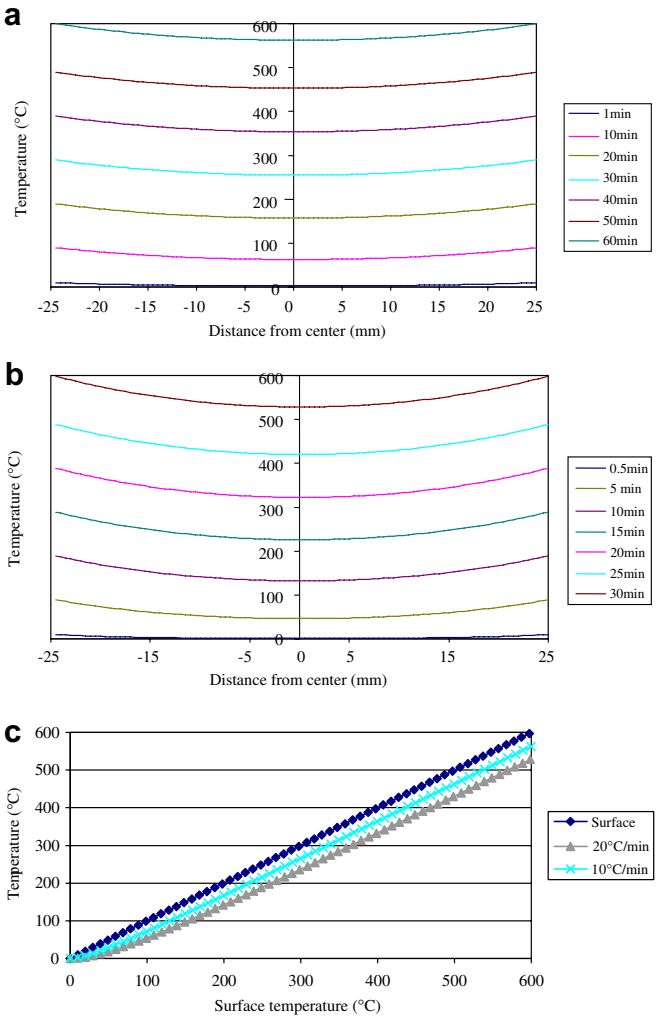

Fig. 3. Temperature profiles along midsections in Cases 1 and 2. (a) Case 1 (heating rate = 10 °C/min); (b) Case 2 (heating rate = 20 °C/min); (c) temperature development at specimens' centers.

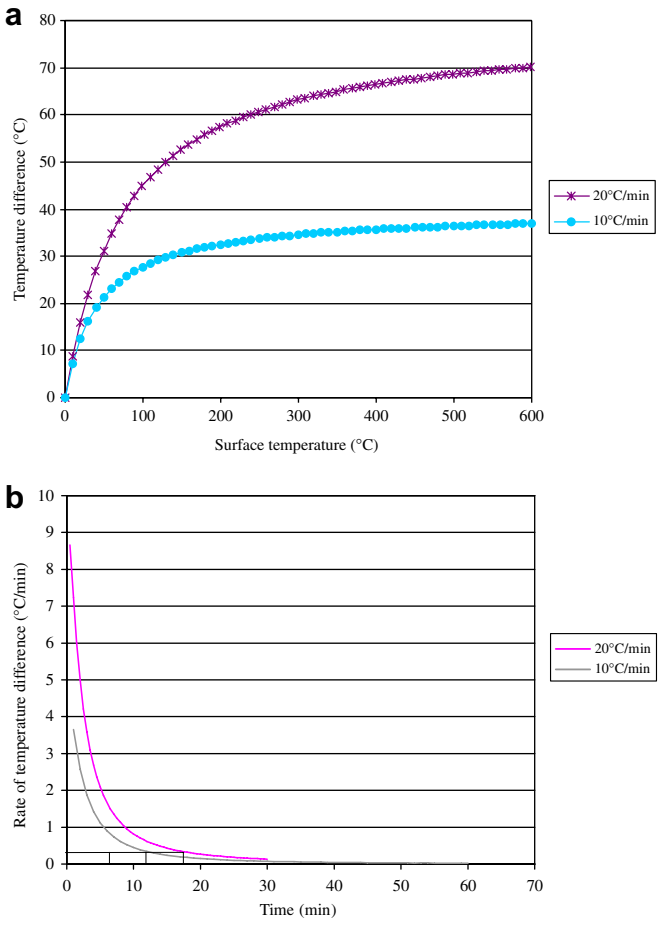

Fig. 4. Increment of temperature difference with time between the center and the surface of specimen in Cases 1 and 2. (a) Temperature difference between the surface and the center of specimen; (b) temperature difference vs. time.

Fig. 4. Temperature difference ΔT gradually reduced or maintained at a constant value in about 12 min after heating for Case "1" as compared to 18 min for Case "2", when the increase rate of temperature difference was less than 0.4 °C/min. Such time is called as "settling time" t_s. It is found that the settling time required for the temperature profile to reach a constant value increased with increasing heating rate. Khoury et al. [6] reported similar results using an analytical method.

4.1.2. Thermal stress fields

Fig. 5 provides information on the corresponding stress fields of Cases "1" and "2". It was found that rapid heating induced substantial tensile stresses at the centers of the numerical specimens due to the imposed thermal gradient. Both σ_x and σ_y were in tension at the center of specimen, and the absolute value of vertical stress σ_y was greater than that of horizontal stress σ_x. The stress σ_y at the surface turned to be compressive; while the stress σ_x approached zero. For these specimens, the stresses σ_y were equal to zero

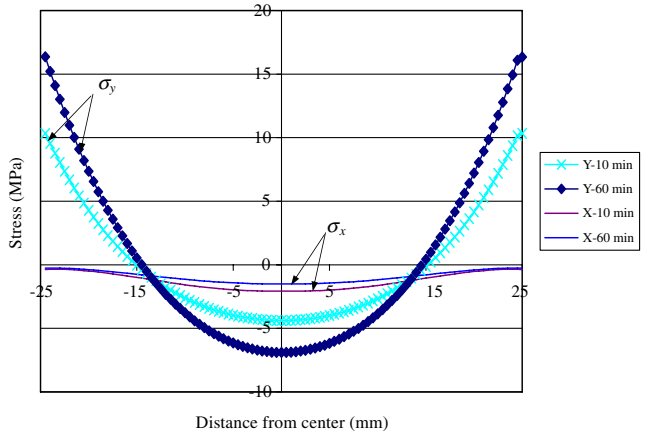

Fig. 5. Thermal stress profiles in Case 2.

at $r = 15$ mm. These results are similar to those reported by Parrott [24].

The thermal stresses in Case "2" were higher than those in Case "1" (see Fig. 6). This was because the higher heating rate caused larger temperature differences ΔT between

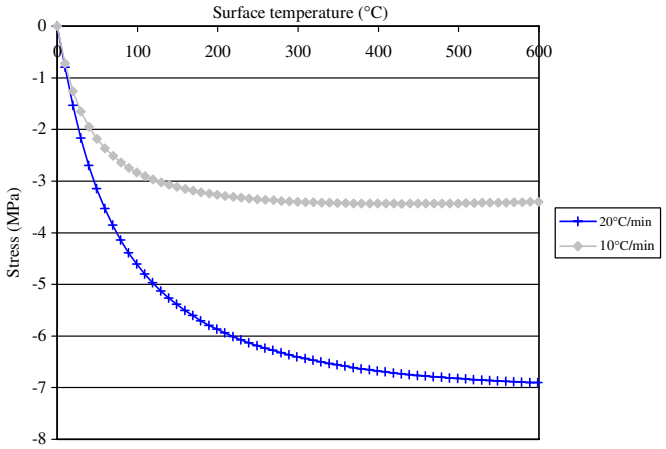

Fig. 6. Thermal stresses vs. surface temperature in Cases 1 and 2.

the surface and the center of the specimen, as shown in Fig. 4a. Their magnitudes increased gradually till the settling time t_s is reached, and then became constant due to a uniform increase of temperature.

4.1.3. Thermal cracking

Fig. 7 shows the thermal cracking process in Case "4" (under the heating rate of 20 °C/min, and constant CTE). Since the stress σ_y was much higher than σ_x, a horizontal crack was first formed at the central region of the specimen when the temperature at the sides (surface) reached 200 °C. With increasing temperatures, the cracks gradually propagated towards the sides (surfaces) of the specimen, but they did not split the concrete specimen. Such cracks can be called as "temperature gradient-induced cracks".

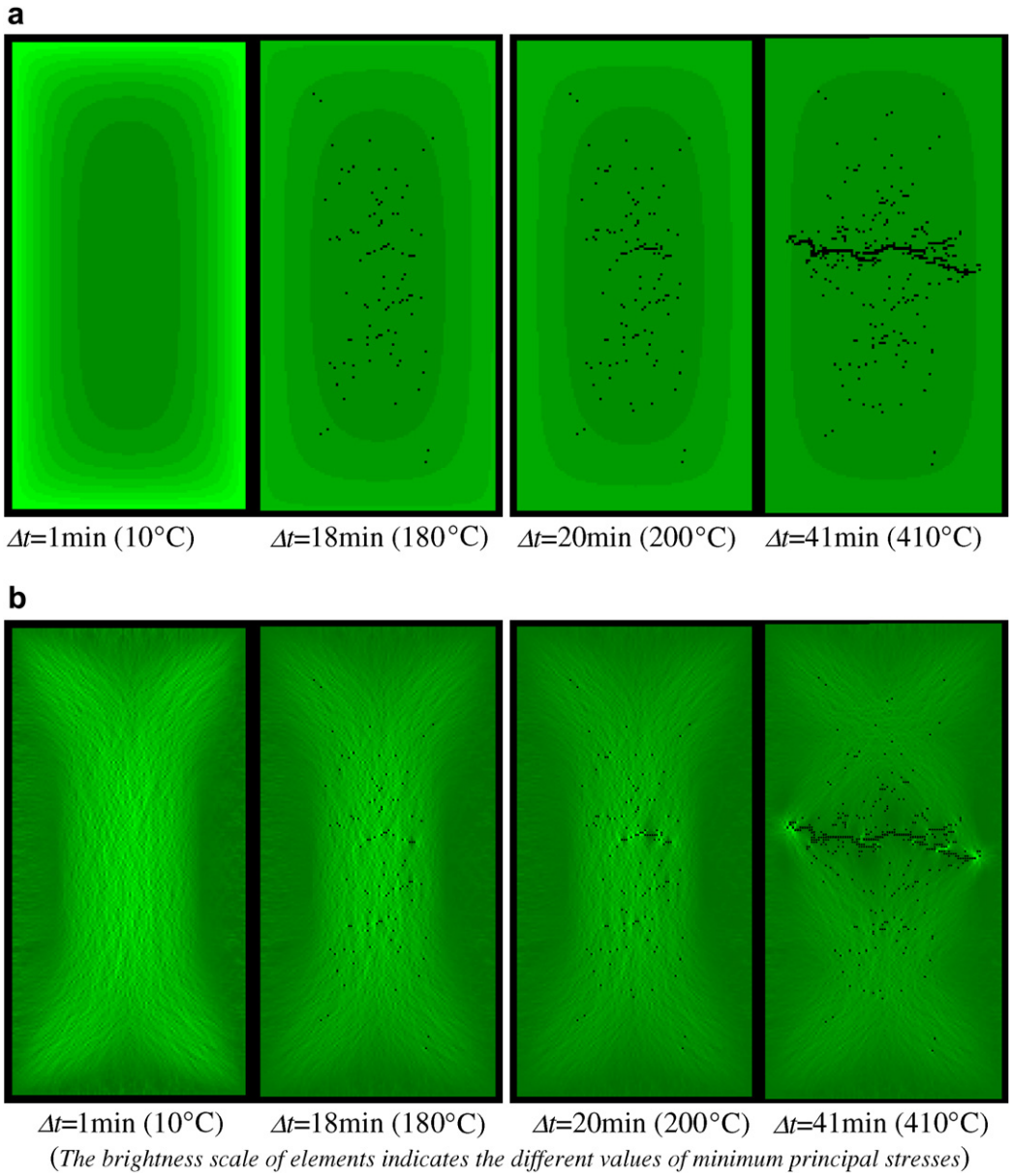

Fig. 7. Thermal gradient and internal cracks in Case 4 (heating rate=20 °C/min). (a) Temperature field in Case 4; (b) thermal stress field and thermal cracking process.

Case "5" simulated the crack formation of a single phase material, like a hardened cement paste which expands at a lower temperature and shrinks at a high temperature. As shown in Fig. 8a, tensile stresses initiated not only at the centre of the specimens, but also along the sides (surface) of the specimen. Consequently, a few cracks appeared in the central region, and more cracks formed on the specimen surface and propagated towards centre of the specimen. These numerical results are similar to the experimental observations reported by Xu et al. [25].

Relationships between the temperature difference ΔT and the crack length of Cases "3", "4" and "5" are compared in Fig. 9. For Case "4", the specimen exhibited a sudden increase in crack length (a rapid propagation of cracks) at the surface temperature of 400 °C. Such a behavior was also found in the specimen of Case "5" at the surface temperature of 220 °C. The lower temperature for the latter case was due to the formation of thermal cracks on the surface of the specimen caused by the shrinkage of the material at high temperatures. It was also noted that the time attending these temperatures was approximately equal to the settling time of the respective specimens. After the settling time, the temperature increment (or the temperature gradient in the specimen was more or less constant). Subsequently, the thermal stress increases were small and the thermal crack propagation ceased. In comparing with Case "4", the growth of crack length of the specimen in Case "3" was relatively gentle over the surface temperatures range between 60 °C and 340 °C. Above 340 °C, the growth of cracks also ceased.

4.2. Cement-based composite with multiple inclusions

4.2.1. Under uniform temperature increment

Fig. 10 shows the thermal cracking induced by the thermal mismatch between the matrix and the inclusion under a uniform temperature increment of 20 °C/min (Case

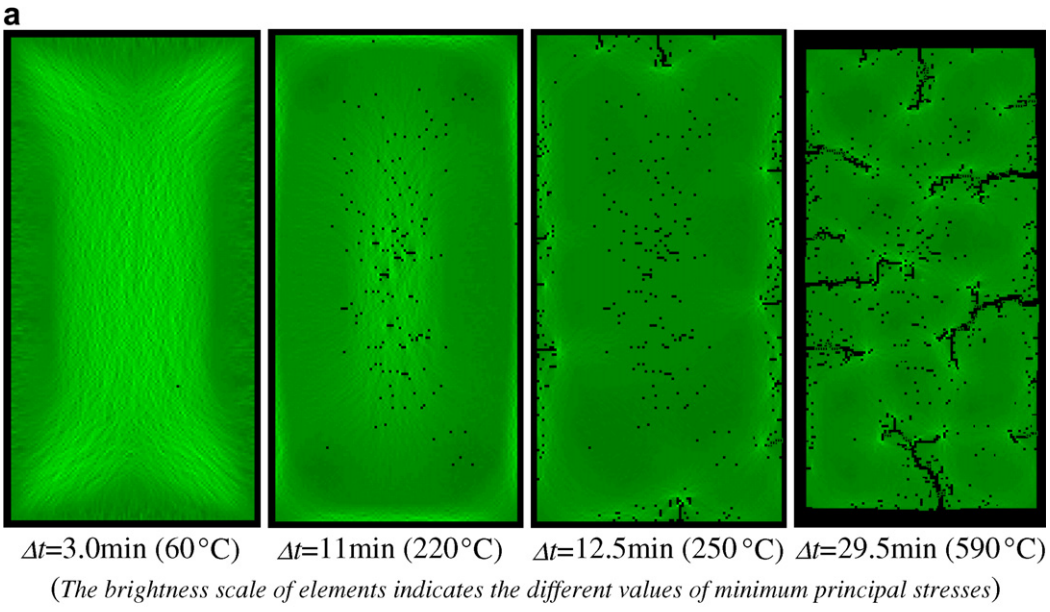

Fig. 8. Thermal stresses and external cracks. (a) Thermally induced external cracks in Case 5 at heating rate of 20 °C/min; (b) thermal cracks on HCP specimens after exposure to 650 °C ([25]).

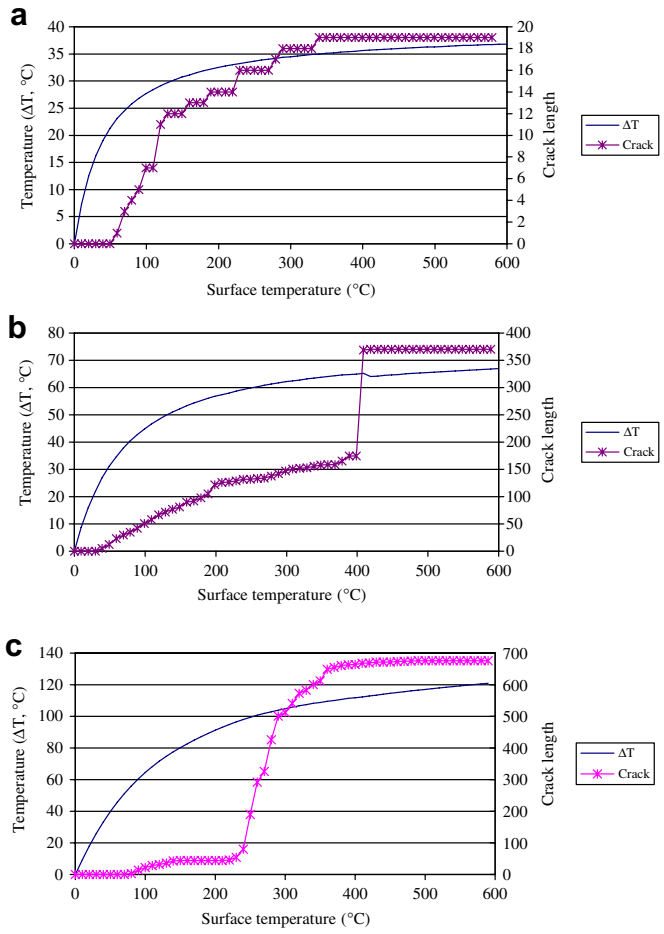

Fig. 9. Relationships between crack length and temperature in Cases 3–5. (a) Case 3 (heating rate = 10 °C/min); (b) Case 4 (heating rate = 20 °C/min); (c) Case 5 (heating rate = 20 °C/min).

"6"). Since the CTE of the inclusion was greater than that of the matrix, the radial cracks were caused by the bursting tangential stresses, which had been described in detail in our previous papers [11,12]. The crack length curve reflected a gradual and slow increase in the number of broken elements with increasing temperatures (see Fig. 12a). It was because the cracks stop extending when they touched the stronger inclusions under each temperature increment.

4.2.2. Under transient thermal loading

Fig. 11 provides information on the effects of the transient thermal loading of 20 °C/min on the thermal cracking of the specimen with multiple inclusions (Case "7"). Due to the temperature gradient, the thermal stresses quickly increased and approached the strength of material at the surface temperature of 100 °C (or the center temperature of 55 °C). A large horizontal crack then formed in the central region of the specimen. When the temperature was increased to 220 °C, other small horizontal cracks formed nearby the center crack. The large center crack slowly developed further both in the matrix and in the inclusion till the settling time t_s was reached. After the settling time, the increment in the temperature difference between the surface and the center became smaller, and the crack development slowed down. Fig. 12b shows a sudden increase of crack length when the temperature difference reached 45 °C (surface temperature of 100 °C), whereas that was not observed in Case "6". The radial cracks induced by the thermal mismatch between the matrix and the inclusions occurred around the inclusions, and are called as thermal mismatch-induced cracks.

The crack propagations in Case "8" were similar to those in Case "7" (see Figs. 12b and c). Below 240 °C, small cracks occurred around the inclusions and a temperature gradient-induced crack appeared in the middle of the specimen. Above 240 °C, the cracks stop extending because: (1) the increase in the temperature difference

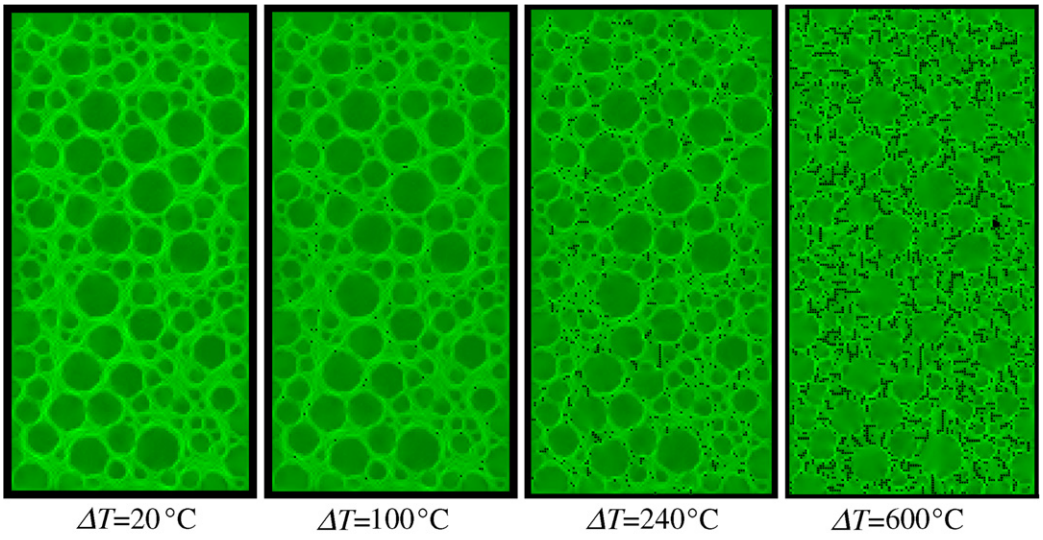

Fig. 10. Thermal cracking process in Case 6 with multiple inclusions under uniform temperature field (temperature increment of 20 °C/min).

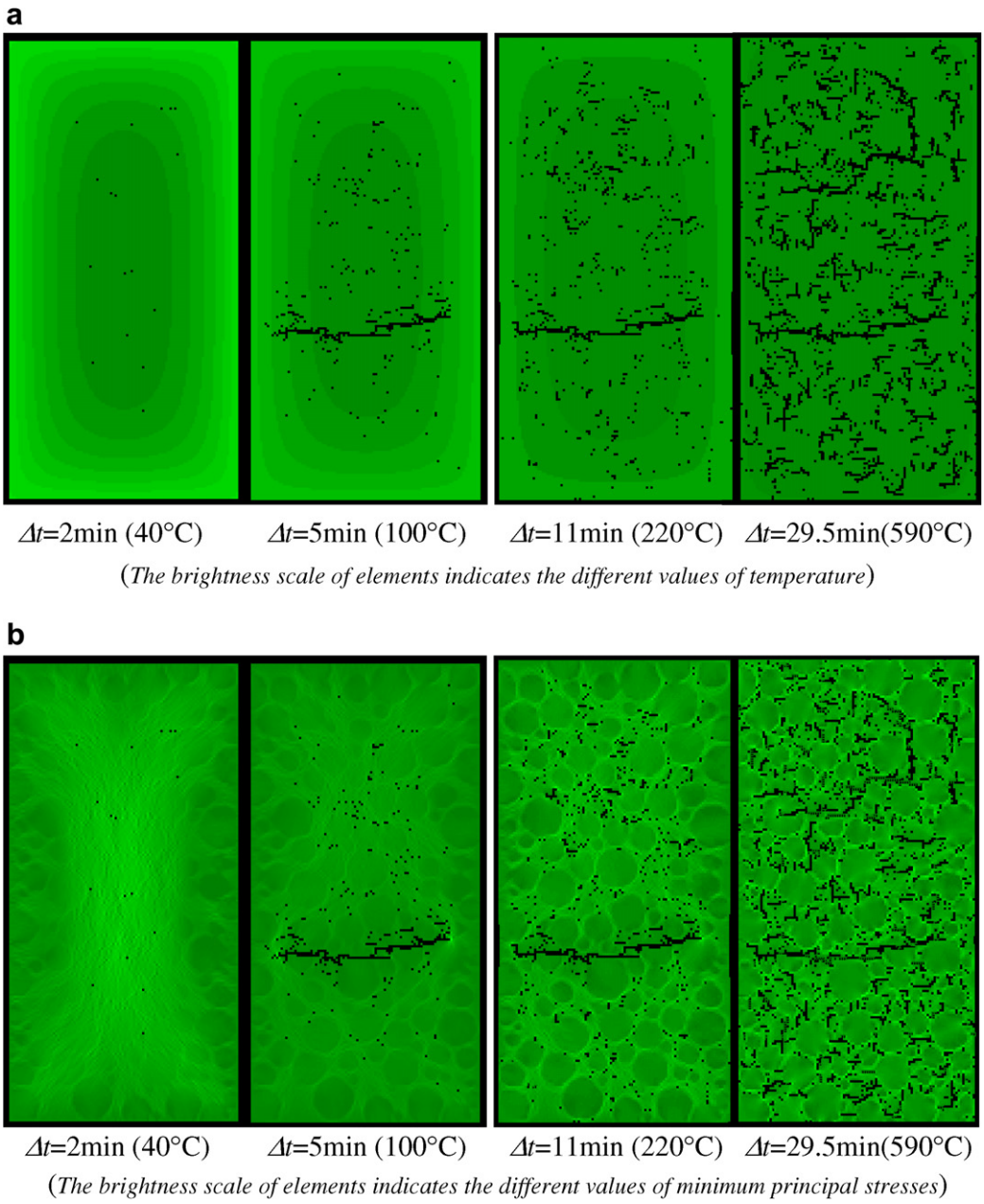

Fig. 11. Thermal gradient and cracking process in Case 7 with multiple inclusions under transient thermal loading (heating rate=20 °C/min). (a) Temperature field in Case 7; (b) thermal stress field and thermal cracking process.

slowed down, and (2) the elastic modulus of the matrix material and the inclusion material decreased. Beyond 460 °C, an increase in the crack length was observed as a result of extending radial cracks around the inclusions. This was mainly due to the thermal mismatch between the matrix and the inclusions.

4.3. Crack patterns

In the present numerical simulations, two categories of cracks were observed: (1) temperature gradient-induced crack and (2) thermal mismatch-induced crack, as shown in Fig. 13. The former can be sub-divided into two kinds: internal cracks and external cracks, according to the location of cracking. If the matrix material expanded with increasing temperature, the temperature gradient-induced cracks initiated in the central region of specimen and propagated to the specimen surface, for example the thermal cracks in concrete. If the matrix material contracted with increasing temperature, temperature gradient-cracks would form on the specimen surface and then developed to the interior, such as the thermal cracks in HCP. The initiation and propagation of temperature gradient-induced cracks were dependent on the temperature difference and the CTE of matrix material. On the other hand, a thermal mismatch-induced crack was attributed into the thermal

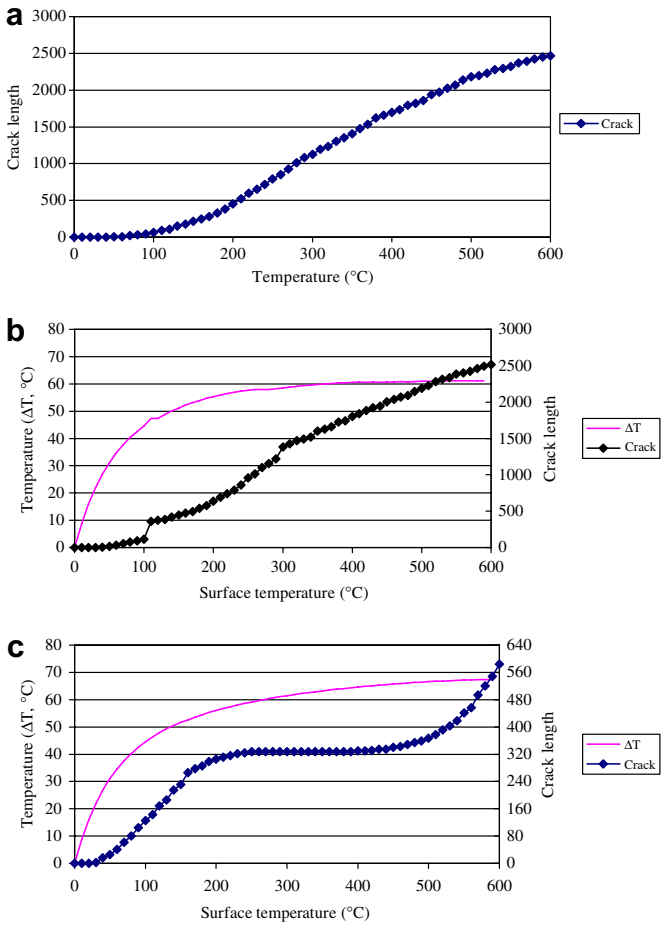

Fig. 12. Relationships between crack length and temperature in Cases 6–8. (a) Case 6 under uniform temperature field; (b) Case 7 under temperature gradient at heating rate of 20 °C/min (c) Case 8 under temperature gradient at heating rate of 20 °C/min.

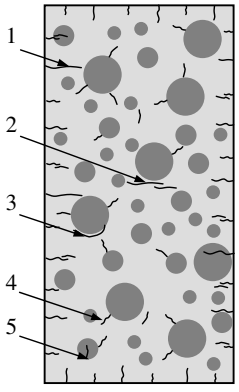

1-Temperature-induced shrinking crack;
2-Temperature gradient-induced horizontal crack;
3-Tangential crack; 4-Radial crack; 5-Inclusion crack

Fig. 13. Crack patterns in cement-based composites at elevated temperatures.

mismatch between the matrix material and the inclusion material, regardless of the temperature gradient. Three types of thermal mismatch cracks were identified. They are the radial cracks, tangential cracks and inclusion cracks [11,12].

5. Discussions on numerical results

Kristensen et al. [8] reported that the internal cracks in concrete exposed to a transient thermal load were more difficult to be detected than the cracks in HCP due to the fact that the internal cracks in concrete were seldom visible on the surfaces of the specimens. They also explained the possible crack formation mechanisms in view of the non-homogeneity and ductility of concrete. In fact, the crack propagation was greatly dependent on the thermal stresses. The crack should develop further if the stresses increased. Under a transient thermal load, the stress level was directly proportional to the temperature difference (as shown in Fig. 6). If the variation of the temperature difference became too small with time, the development of stress level decreased or stopped even during the heating process (see Fig. 4b). Accordingly, the associated thermal crack propagation slowed down or was arrested. This can be used to explain why there are fewer cracks measured in the concrete under a lower heating rate even the same target temperature is reached.

The explosive spalling of concrete under elevated temperatures is related to the build-up of internal pore water pressure derived from the 'moisture clog' [26]. This explanation is probably suitable for a fully saturated concrete. Chan [16] reported that explosive spalling frequency of concrete depended on both the moisture content and the strength of the concrete (as shown in Fig. 14). For concrete with a compressive strength higher than 60 MPa, the spalling frequency increased with moisture content. Other studies [27–30] revealed that there were uncertainties on concrete spalling occurrence even under controlled conditions (heating regime, mix proportion and moisture content). These uncertainties of experimental results imply that the pore pressure is not the sole factor to induce the explosive spalling.

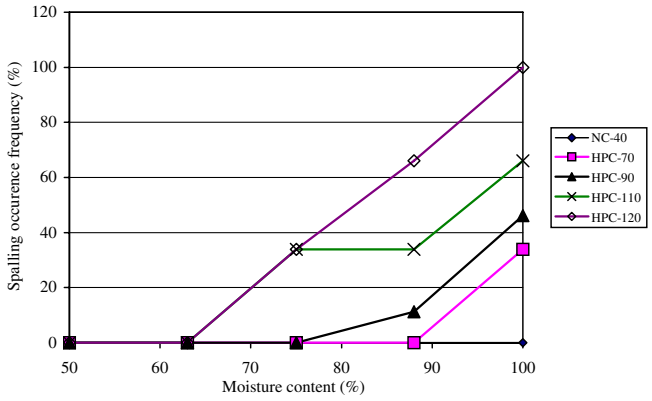

Fig. 14. Probability of spalling occurrence [16].

Making use of the numerical results described in this paper, the uncertainties of explosive spalling can be explained in two aspects: (1) strain energy produced by thermal stresses and pore pressure and (2) thermal cracks in concrete. Cracks play a twofold role in affecting the mechanical properties of concrete subjected to elevated temperatures. The cracks help to increase the permeability of the concrete so that the pore pressure can be released more easily. At the same time, the cracks also weaken the concrete strength.

It is believed that the spalling occurrence is dependent on the pore pressure and on the crack development process, which are closely related to the heating rate and the heterogeneity of the concrete materials. This can be illustrated by a schematic diagram shown in Fig. 15. If the pore pressure is built up more quickly than the rate of crack propagation, explosive spalling would possibly occur. Fig. 16 illustrates a typical fractured concrete specimen after it has experienced explosive spalling. The specimen was split into two fragments at a heating rate of 10 °C/min. It was suggested that horizontal cracks were the trigger of the spalling process. After the cracks were formed as a result of a temperature gradient, the pore pressure speeded up the crack propagation and eventually led to explosive spalling. As discussed in the previous sections, the temperature gradient-induced cracks occurred before the maximum temperature difference was reached, but they did not split up the concrete specimen. This was consistent with the experimental observation that explosive spalling took place when the temperature difference between the surface and the center of the specimen approached a maximum value [30]. On the other hand, the explosive spalling can be avoided if the pore pressure can be released through crack channels. Kalifa et al. [30] pointed out the severe cracks occurred on the specimen surface or in the interior part of the specimen, and they formed paths for vapor to escape.

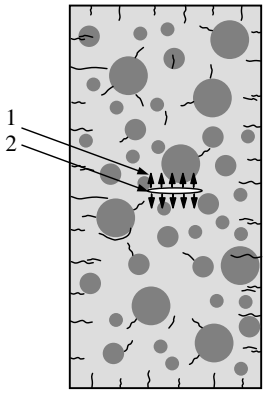

1-Pore water pressure; 2-Temperature gradient-induced crack

Fig. 15. Schematic of explosive spalling mechanism.

Fig. 16. Fractured concrete by explosive spalling (observed in experimental studies conducted at The Hong Kong Polytechnic University, 2003).

6. Conclusions

Based on the results of this study, the following observations are made:

1. The temperature gradient is dependent on the heating rate and the thermal conductivity. The temperature difference ΔT between the surface and the center representing the temperature gradient increases rapidly before the settling time t_s and thereafter approaches a constant value. The settling time t_s increases with the heating rate.
2. Under a temperature gradient, the crack occurrence depends on a certain temperature difference ΔT, at which the thermal stress reaches the strength of material. Most of the thermal cracks induced by temperature gradient occur before the settling time t_s if the temperature difference ΔT is large enough to break the material. Majority of the thermal cracks induced by the thermal mismatch between the HCP and the inclusions take place after the settling time t_s.
3. Under a temperature gradient, the crack patterns in cement-based composite are closely related to the heating rate and the nature of thermal expansions of phase materials. The formation of the internal cracks and the external cracks is due to different mechanisms. For a hardened cement paste, the internal crack is due to the thermal expansion of HCP as well the temperature gradient at lower temperatures. The external crack is due to thermal shrinkage of HCP and the temperature gradient at higher temperatures.
4. The formation and the random propagation of the temperature gradient-induced cracks and the thermal mismatch-induced cracks, together with the existence of pore water pressure are probably the essential factors for the uncertainties of explosive spalling of concrete exposed to elevated temperatures.
5. For a multi-phase cement-based composite, the strong inclusions can efficiently arrest the crack propagation.

This study has not quantified the effects of moisture content, which can substantially affect the cracks induced

by the temperature gradient and the thermal mismatch. The coupling of the thermal cracking and the pore water pressure should be studied in order to have a better understanding of explosive spalling in a quantitative manner. The authors are conducting further work in this direction. Furthermore, in order to realistically model the thermal performance of multi-phase materials, a 3-D FEM program should be developed in future.

Acknowledgement

This research study is supported by The Hong Kong Polytechnic University and the NNSF of China (Grant No. 50408029).

References

[1] Bazant ZP. Review of literature on high-temperature behavior of concrete. Report NL-TM-5145. Oak Ridge National Laboratory, TENN, USA; 1976.
[2] Phan LT. Fire performance of high-strength concrete: a report of the state-of-the-art. NISTIR5934, NIST, USA; 1996.
[3] Diederichs U, Jumpanen UM, Penttala V. Material properties of high strength concrete at elevated temperatures. IABSE 13 Congress, Helsinki; 1988. p. 489–94.
[4] Wong YL. Spalling of concrete under fire. International seminar on recent development of fire protection in structures, The Hong Kong institute of steel construction; 2004. p. 41–51.
[5] Timoshenko SP, Goodier JN. Theory of elasticity. 3rd ed. USA: McGraw-Hill; 1970.
[6] Khoury GA, Sullivan PJE, Grainger BN. Radial temperature distributions within solid concrete cylinders under transient thermal states. Mag Concrete Res 1984;36(128):146–56.
[7] Carslaw HS, Jaeger JC. Conduction of heat in solids. 2nd ed. UK: Clarendon Press; 1959.
[8] Kristensen L, Hansen TC. Cracks in concrete core due to fire or thermal heating shock. ACI Mater J 1994;91(5):453–9.
[9] Bazant ZP, Kaplan MF. Concrete at high temperatures. Longman; 1996.
[10] Khoury GA, Majorana CE, Pesavento F, Schrefler BA. Modelling of heated concrete. Mag Concrete Res 2002;54(2):77–101.
[11] Fu YF, Wong YL, Tang CA, Poon CS. Thermal induced stress and associated cracking in cement-based composite at elevated temperatures. Part I. Thermal cracking around single inclusion. Cement Concrete Comp 2004;26(2):99–111.
[12] Fu YF, Wong YL, Tang CA, Poon CS. Thermal induced stress and associated cracking in cement-based composite at elevated temperatures. Part II. Thermal cracking around multiple inclusions. Cement Concrete Comp 2004;26(2):113–26.
[13] Sarshar R, Khoury GA. Materials and environmental factors influencing the compressive strength of unsealed cement paste and concrete at high temperatures. Mag Concrete Res 1993;45(162):51–61.
[14] Macvean DB, Alblas JB. Thermoelasticity. The Netherlands: Wolters-Noordhoff; 1969.
[15] Hsu TR. The finite element method in thermomechanics. USA: Allen & Unwin; 1986.
[16] Chan YN, Peng GF, Anson M. Fire behavior of high-performance concrete made with silica fume at various moisture contents. ACI Mater J 1999;96(3):405–11.
[17] Wang KJ, Jansen DC, Shah SP. Permeability study of cracked concrete. Cement Concrete Res 1997;27(3):381–93.
[18] Krajcinovic D. Damage mechanics. The Netherlands: Elsevier Science; 1996.
[19] Fu YF, Wong YL, Poon CS, Tang CA, Lin P. Experimental study of micro/macro crack development and stress–strain relations of cement-based composite materials at elevated temperatures. Cement Concrete Res 2004;34:789–97.
[20] Mazars JA. Description of micro- and macro-scale damage of concrete structures. Eng Fracture Mech 1986;25(5/6):729–37.
[21] Yu TQ. Linear damage model of separation function for concrete. Key Eng Mat 1982;2:14–6 [in Chinese].
[22] Logan DL. A first course in the finite element method using Algor. USA: University of Wisconsin-Platteville, Brooks/Cole, Thomson Learning, Inc.; 2001.
[23] Fu YF. Thermal stresses and associated damage in concrete at elevated temperatures. PhD thesis, The Hong Kong Polytechnic University, Hong Kong; 2003.
[24] Parrott LJ. A study of transitional thermal creep in hardened cement paste. Mag Concrete Res 1979;31(107):99–103.
[25] Xu YG, Wong YL, Poon CS, Anson M. Impact of high temperature on PFA concrete. Cement Concrete Res 2001;31(7):1065–73.
[26] Harmarthy TZ. Effect of moisture on the fire endurance of building elements. Philadelphia: ASTM Publication STP; 1965. 74–95.
[27] Furumura F, Abe T, Shinohara Y. Mechanical properties of high strength concrete at high temperatures.In: Proceedings of the fourth Weimar workshop on high performance concrete: material properties and design. Weimar, Germany; 1995. p. 237–54.
[28] Hammer TA. High-strength concrete phase 3: compressive strength and E-modulus at elevated temperatures. SP6 fire resistance, Report 6.1, SINTEF structures and concrete; 1995.
[29] Kalifa P, Menneteau FD, Quenard D. Spalling and pore pressure in HPC at high temperatures. Cement Concrete Res 2000;30:1915–27.
[30] Phan LT, Lawson JR, Davis FL. Effects of elevated temperature exposure on heating characteristics, spalling, and residual properties of high performance concrete. Materials Struct 2001;34:83–91.